Unconventional Flatband Line States in Photonic Lieb Lattices

Shiqi Xia,[1] Ajith Ramachandran,[2,‖] Shiqiang Xia,[1] Denghui Li,[1] Xiuying Liu,[1] Liqin Tang,[1] Yi Hu,[1] Daohong Song,[1,3,*] Jingjun Xu,[1,3] Daniel Leykam,[2,†] Sergej Flach,[2,‡] and Zhigang Chen[1,3,4,§]

[1]*The MOE Key Laboratory of Weak-Light Nonlinear Photonics, TEDA Applied Physics Institute and School of Physics, Nankai University, Tianjin 300457, China*

[2]*Center for Theoretical Physics of Complex Systems, Institute for Basic Science (IBS), Daejeon 34126, Republic of Korea*

[3]*Collaborative Innovation Center of Extreme Optics, Shanxi University, Taiyuan, Shanxi 030006, China*

[4]*Department of Physics and Astronomy, San Francisco State University, San Francisco, California 94132, USA*

(Received 12 April 2018; published 28 December 2018)

Flatband systems typically host "compact localized states" (CLS) due to destructive interference and macroscopic degeneracy of Bloch wave functions associated with a dispersionless energy band. Using a photonic Lieb lattice (LL), such conventional localized flatband states are found to be inherently incomplete, with the missing modes manifested as extended *line states* that form noncontractible loops winding around the entire lattice. Experimentally, we develop a continuous-wave laser writing technique to establish a finite-sized photonic LL with specially tailored boundaries and, thereby, directly observe the unusually extended flatband line states. Such unconventional line states cannot be expressed as a linear combination of the previously observed boundary-independent bulk CLS but rather arise from the nontrivial real-space topology. The robustness of the line states to imperfect excitation conditions is discussed, and their potential applications are illustrated.

DOI: 10.1103/PhysRevLett.121.263902

Flatband systems, first proposed for the study of ferromagnetic ground states in multiband Hubbard models, have been proven to be conceptually effective and important in condensed matter physics [1–3]. They are characterized by a band structure with one band being completely flat, signaling macroscopic degeneracy. One can construct compact localized states (CLS) which remain intact during evolution due to destructive interference. Over the years, a variety of approaches have been developed to design and characterize different flatband systems [4–8] with various lattice geometries [7–12]. This is in large part because the flatband systems provide a platform for probing various fundamental phenomena that have intrigued scientists for decades, including Anderson localization [6,13,14], nontrivial topological phases and quantum Hall states [15–19], and flatband superfluidity [20,21].

The Lieb lattice (LL)—a face-centered depleted square lattice [Fig. 1(a)]—is geometrically different from other two-dimensional lattices such as square and honeycomb lattices. This peculiar system possesses a single conical intersection point in its Brillouin zone (BZ), where the flatband is sandwiched between two conical Bloch bands [Fig. 1(b)]. The flatband in the LL is protected by a chiral symmetry, and its intersection with the dispersive bands is protected by real-space topology [12,22,23]. Recently, LLs have been realized in several different settings, including Bose-Einstein condensates [4,24], surface state electrons [25,26], exciton polaritons in micropillars [27], and waveguide arrays in photonic structures [28–32]. However, so far most previous experimental studies have focused on the demonstration of the LL structures and their associated CLS, overlooking unusual features that arise in infinitely extended lattices [Fig. 1(c)] or finite (truncated) lattices with different cutting boundaries [Figs. 1(d) and 1(e)].

In this Letter, we demonstrate the CLS previously investigated in the LL are linearly dependent, so they do not form a complete basis for the flatband. The missing states completing the flatband basis are unconventional line states, which *cannot* be formed by linear superpositions of the conventional boundary-independent bulk CLS [23]. Such line states exist in principle only in the infinite LL, or wrap around the lattice under periodic boundary conditions, forming noncontractible loops. However, with an appropriate termination of the lattice, these line states can be observed even in a finite system. Experimentally, we develop a simple yet effective writing technique with a weak continuous-wave laser (rather than a high-power femtosecond laser) to establish finite-sized photonic LL with the desired boundaries. More importantly, we demonstrate the existence of the line states (and their variation in other shapes) in the truncated LL from direct measurements of both real-space intensity and the

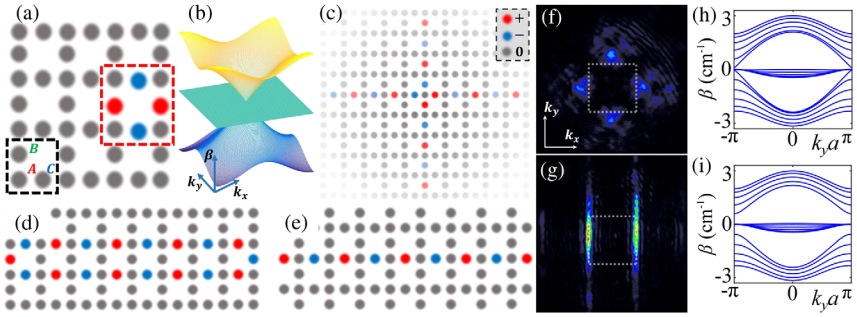

FIG. 1. Flatband states in a photonic LL. (a) Illustration of lattice structure consisting of three sublattices (A, B, C) shown as a dark-dashed square, with a flatband mode (the CLS) shown as a red dashed square. Sites with zero amplitudes are denoted by gray dots, and those with nonzero amplitudes of opposite phase by red and blue dots. (b) Calculated band structure in the first BZ. (c) Two line states illustrated in an *infinite* LL. (d) A necklace-shaped flatband state in a *finite* LL with flat edges. (e) A unconventional line state in a finite LL with bearded edges. (f),(g) Measured k-space spectrum of (f) the CLS and (g) the line state. (h),(i) Band structure for a semi-infinite LL with (h) flat and (i) bearded edges.

momentum-space spectrum. The robustness of these unconventional line states to imperfect excitation conditions is also discussed, along with specific examples of their potential applications.

Propagation of a light beam along the LL composed by evanescently coupled identical optical waveguides [sketched in Fig. 1(a)] is described by the paraxial wave equation [32,33]:

$$\frac{\partial}{\partial z}\psi(x,y,z) = \left(\frac{i}{2k}\nabla_\perp^2 + \frac{ik}{n_0}\Delta n(x,y)\right)\psi(x,y,z), \quad (1)$$

where $\psi(x,y,z)$ is the envelope of the electric field, $k = 2\pi n_0/\lambda$ is the wave number, λ is the wavelength, n_0 is the bulk refractive index, $\Delta n(x,y)$ is the optically induced refractive index lattice, and $\nabla_\perp^2 = \partial_x^2 + \partial_y^2$ is the transverse Laplacian. Under the tight-binding approximation, this model reduces to the well-known linear discrete Schrödinger equation [28–31,33]. For the LL, eigenvalue equations can be explicitly written for wave amplitudes in the unit cell denoted by (n,m) as

$$\begin{aligned} \beta A_{n,m} &= B_{n,m} + B_{n,m-1} + C_{n,m} + C_{n-1,m}, \\ \beta B_{n,m} &= A_{n,m} + A_{n,m+1}, \quad \beta C_{n,m} = A_{n,m} + A_{n+1,m}. \end{aligned} \quad (2)$$

A plane wave ansatz for the eigenvectors with momenta (k_x,k_y) yields the band structure: $\beta_{\mathrm{FB}} = 0$, $\beta(k_x,k_y) = \pm\sqrt{2}[2+\cos(k_x)+\cos(k_y)]^{1/2}$. A zero energy flatband touches two linearly dispersive bands intersecting at the conical intersection point as shown in Fig. 1(b). Normally, modes in the continuum are not localized, except for those generated under special conditions as "bound states in the continuum" [34–36]. The flatband supports inherently degenerated CLS that have a nonzero amplitude only at four lattice sites as shown in Fig. 1(a), where all A sites (the minority sites) have a zero amplitude but B and C sites (the majority sites) have a nonzero amplitude with opposite phase. Such a solution satisfies Eq. (2) at $\beta = 0$. These states are not only localized but also compact, residing in only three unit cells. Other localized states (such as necklace-shaped flatband states) can be established by linear combinations of the CLS, as demonstrated in previous experiments [30–32]. However, in certain lattices where the flatband intersects other dispersive bands, the set of CLS can become linearly dependent under periodic boundary conditions—i.e., an appropriate superposition of all the CLS vanishes—and consequently they do not form a complete basis for the flatband [23]. The missing states which complete the flatband basis are the *line states*, which are extended across the entire lattice. Such line states also satisfy conditions for destructive interference, and their associated wave functions represent exact eigenstates at the flatband energy $\beta = 0$. A line state solution of Eq. (2) elongated in the y direction is given by $B_{n,m} = -B_{n,m+1}$ for a given n, with all other amplitudes in Eq. (2) vanishing. Likewise, a line state elongate in the x direction is given by $C_{n,m} = -C_{n+1,m}$ for a given m, and all other amplitudes vanish. These states cannot be expressed as a linear combination of the CLS shown in Fig. 1(a). For an infinite lattice (or a lattice with periodic boundary condition folds into a 2D torus), there are only two distinct line states as illustrated in Fig. 1(c), and all other line states can be obtained by discrete translation or combination. For an experimentally feasible finite-sized LL, the termination of the lattice boundaries determines whether a particular line state can exist. For the "flat" edges shown in Fig. 1(d), only the necklace-shaped state is allowed, but this state can be expressed as a linear superposition of the CLS. Linearly independent line states do not exist, and the CLS form a complete basis under this edge condition. On the other hand, by cutting the lattice to form "bearded" edges [37], the line state terminates smoothly at the boundaries [Fig. 1(e)]. In this latter case, the line shape can be efficiently kept, but the state cannot be expressed as a superposition of the CLS. The k-space spectra are measured and displayed in Figs. 1(f)

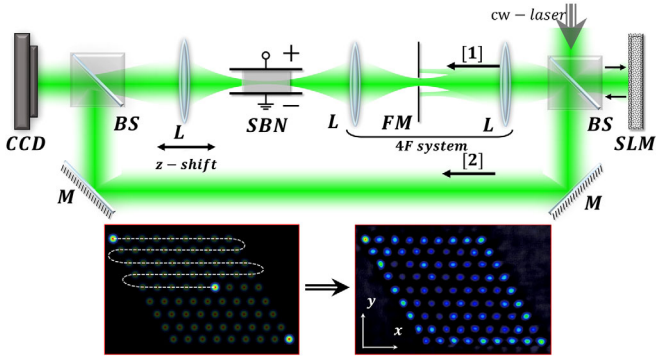

FIG. 2. Experimental setup for site-to-site writing of photonic lattices with a cw laser in a nonlinear crystal. SLM, spatial light modulator; BS, beam splitter; FM, Fourier mask; SBN, strontium barium niobate. Path 1 is for both writing and probe beams, and path 2 is for the interference reference beam. Bottom left: Sequential positions of the writing beam. Bottom right: A typical photonic lattice written in the crystal as probed by a broad (quasi-plane-wave) beam.

and 1(g), where the white dashed square marks the edge of the first BZ. The spectrum of the CLS is distributed around the four sides of the first BZ, whereas that of the line state is mainly along the two zone edges. In Figs. 1(h) and 1(i), a band structure calculation using the paraxial equation is shown for a semi-infinite lattice, illustrating the existence or absence of edge states depending on the lattice termination. The boundary-dependent superposition of the CLS in finite LL is detailed in Supplemental Material [38], emphasizing the linear dependence (independence) of the CLS for the bearded (flat) edges [12].

To observe the extended flatband states, we introduce a simple cw laser writing technique to establish the finite-sized photonic LL with desired boundaries. The technique relies on site-to-site inducing or writing waveguides in a nonlinear photorefractive (SBN) crystal. Different from previous methods [28–32], the LL written in the crystal can be readily reconfigurable with virtually arbitrary lattice edges. Figure 2 shows a schematic of the experimental setup. A cw laser beam ($\lambda = 532$ nm) with only 50 mW power is used to illuminate an SLM, which creates a writing beam with reconfigurable input positions. The 4F system (combination of two lenses) guarantees a quasinondiffracting zone of the beam as it propagates through the 10-mm-long crystal. Because of the noninstantaneous self-focusing nonlinearity, all waveguides remain intact within the one-by-one writing and data acquisition period. The bottom panels in Fig. 2 illustrate the writing principle and a typical triangular lattice. (A nondiffracting Bessel beam can also be used to write the waveguides, but the side lobes of the Bessel beam can affect the lattice structure [39].)

After this proof of principle, we employ the technique to write photonic LL with the desired lattice edges. Figure 3(a) shows such a laser-written LL with bearded edges. The lattice spacing is about 32 μm. With controlled writing beam intensity and exposure time, the waveguide coupling occurs mainly between nearest neighbors, satisfying the tight-binding model. Indeed, after propagating through the 10 mm crystal, a single-site excitation leads to discrete diffraction and coupling mainly to the nearest waveguides [see the inset in Fig. 3(a)]. To observe the extended flatband line states displayed in Fig. 1(e), the input probe beam is shaped into a dotted line pattern, with its phase modulated by the SLM so that adjacent "pearls" have opposite phase [Fig. 3(b1)]. Without the lattice, the line shape cannot be preserved after free propagation due to interference between pearls and diffraction of each pearl [Fig. 3(b2)]. In contrast, when such a line beam is launched into the LL [see Fig. 3(a) for its input position], its overall intensity pattern is well maintained [Fig. 3(b3)]. Furthermore, each pearl remains localized and out of phase with its neighbors as verified from the interferogram [Fig. 3(b4)], in agreement with the predictions. For direct comparison, corresponding results for an in-phase line beam

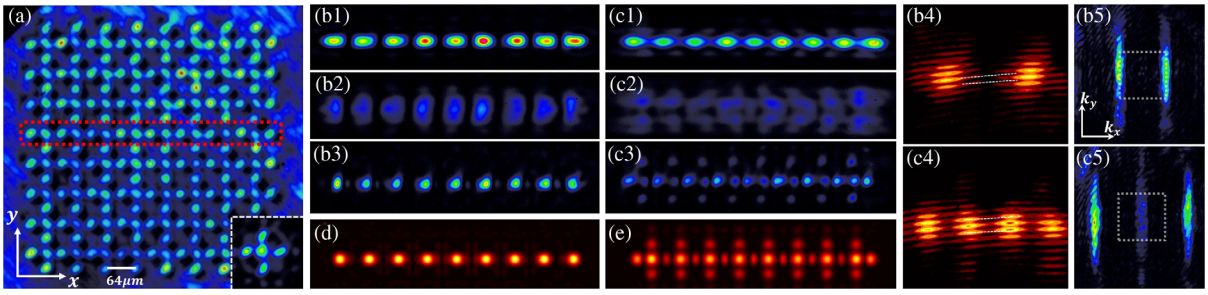

FIG. 3. Demonstration of unconventional line state in a photonic LL with bearded edges. (a) LL established with the cw laser writing technique. A red dashed square marks the input position of the line-shaped probe beam (the inset shows a discrete diffraction of single-site excitation). (b1)–(b3) Transverse intensity pattern of out-of-phase beam at (b1) input, (b2) output without LL, and (b3) output through LL as a propagation-invariant eigenstate. (b4) Separate enlargement interferogram of the output pattern with a reference beam showing adjacent pearls in the line beam are out of phase (white dashed lines added for visualization). (b5) Measured k-space spectrum of (b3) with a dashed square marking the first BZ. (c1)–(c5) The same as in (b1)–(b5) except that all sites are now in phase. (d), (e) Simulation results showing the out-of-phase line state remains intact but the in-phase one deforms strongly after propagating a distance of 4 cm through the lattice.

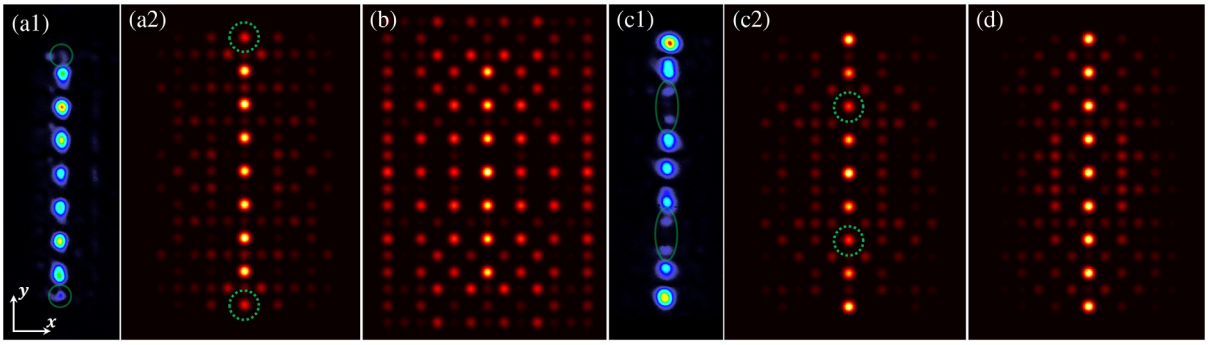

FIG. 4. Line states under imperfect excitation conditions. (a),(b) A shorter line not extending to the LL boundary tends to evolve into a line state with bearded edges [(a1) from experiment; (a2) from simulation] but delocalized with flat edges (b). (c),(d) A self-healing line state under an imperfect amplitude (two defects) [(c1) from experiment; (c2) from simulation] or imperfect phase ($3\pi/4$) between adjacent sites (d). The green dashed circles mark the initial empty sites. Restoration of the line state is not complete in (a1) and (c1) due to the limited propagation distance.

(when all pearls are made with equal phase) are presented in Figs. 3(c1)–3(c3). In this latter case, the line becomes deteriorated, as energy couples to zero-amplitude lattice sites [Fig. 3(c3)], although the in-phase feature is still preserved [Fig. 3(c4)]. Moreover, a dramatic difference is observed in the k-space spectrum between the out-of-phase and in-phase line beams [Figs. 3(b5) and 3(c5)]: The spectrum of the out-of-phase line is distributed along the BZ edges, whereas that of the in-phase one goes to the center of the first BZ, although tunneling to higher BZs is present in both cases because of coupling to dispersive bands in the finite LL. Because of the short propagation distance limited by the crystal length in the experiment, we perform a numerical simulation to further corroborate the experimental observations. Results with parameters similar to our experiments but for a much longer propagation distance (40 mm) are presented in Figs. 3(d) and 3(e). One can see clearly the difference between the out-of-phase beam (remains intact as unconventional line states) and in-phase beam (becomes strongly distorted). Following a similar approach, we also generated a photonic LL with flat edges and demonstrated the necklace-shaped flatband states illustrated in Fig. 1(d). These results and relevant discussions are provided in Supplemental Material [38].

To illustrate the robustness of the line states to imperfect excitation conditions in the LL, we perform additional experiments and numerical simulations based on the tight-binding model. Typical results are presented in Fig. 4. A "shorter" line (not winding around all the way to the lattice edges) tends to extend and couple its energy to the two bearded edges to form the line state [Figs. 4(a)], but it cannot preserve in the LL with flat edges as its energy couples more to the direction perpendicular to the line rather than along the line [Fig. 4(b)]. These results show that the line states are boundary-dependent eigenstates, quite different from the conventional CLS, as discussed further in Supplemental Material [38]. Fully extended lines with an "imperfect" initial phase or amplitude can still evolve into "self-healing" line states [Figs. 4(c) and 4(d)]. Of course, if the input conditions deviate too much from that of the line states, the dispersive band modes are excited most, which leads to a strong discrete diffraction in the lattice.

Before closing, we elaborate on potential applications of these unconventional flatband line states. Conventional CLS can be useful for image transmission in the LL but only limited to a certain necklace-like shape as a superposition of "ring modes" [32]. By combining the features of the CLS and the new line states, it is possible to realize large-scale image transmission with virtually any patterns extended to lattice boundaries [40]. To illustrate this, we transmit three different letters ("PRL") based on the combination of the line states and the CLS in the bearded LL, as shown in Fig. 5. All three letters consist of out-of-phase points, terminating on the bearded edges [Fig. 5(a)]. The shape of the letters preserves after propagation through the lattice, as observed in the experiment [Fig. 5(b)]. A numerical simulation to a longer propagation distance (40 mm) leads to a dramatic difference for a direct comparison between the out-of-phase and in-phase letters [Figs. 5(c) and 5(d)]. The measured output $\boldsymbol{k}$-space spectra for all three letters are qualitatively similar (only the spectrum of the letter L is shown in the insets), distributing mainly along the first BZ edges for the out-of-phase letters (i.e., based on the flatband states) but splitting into the center and higher zones for the in-phase letters where modes of dispersive bands are excited. Another example is related to tunable conductivity. As shown in the band structure for a semi-infinite LL [Figs. 1(h) and 1(i)], nanoribbons can be made conducting or insulating. Moreover, the state in Fig. 1(d) could be destroyed by a vertical potential gradient (electric field), while the state in Fig. 1(e) would be completely unaffected. Therefore, nanoribbons formed from an artificial LL can be either metallic (gapless) or semiconducting (gapped), depending on the edge termination. This generalizes the behavior of graphene nanoribbons. By tuning the potential of the edge sites, one may switch between metallic and semiconducting regimes or "pump" modes between the two bulk bands.

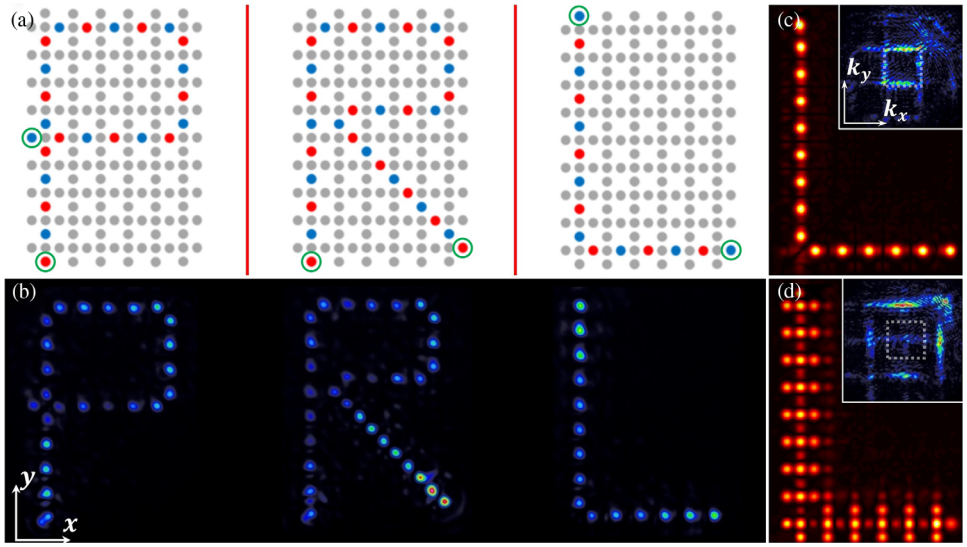

FIG. 5. Demonstration of text transmission based on flatband line states. (a) Schematic of the input letters PRL in a bearded Lieb lattice, with the ending sites marked by green circles. (b) Experimental results of output letters after propagating through the lattice. (c), (d) Numerical simulation to a propagation distance (4 cm) for a direct comparison between (c) out-of-phase and (d) in-phase letter L, where the insets show the measured Fourier spectrum for the letter L from the experiment.

In conclusion, we have demonstrated unconventional flatband line states in a photonic LL "fabricated" with desired boundaries. Our experimental results are further corroborated by numerical simulations based on the paraxial wave equation, while the robustness of the line states to imperfect excitation conditions is analyzed with the coupled mode theory. Our work demonstrates that a reconfigurable platform of designer photonic lattices could bring about numerous opportunities for both fundamental studies and potential applications. For example, the unconventional flatband states may prove relevant to similar phenomena in other flatband systems in condensed matter physics. Moreover, our technique for writing special lattices could be useful for the study of a number of intriguing phenomena such as edge states and topological phases, singularity character and flatband topology, and nonlinear topological solitons [27,41–44].

This work is supported by the National Key R&D Program of China (2017YFA0303800), National Natural Science Foundation of China (91750204, 11704102, and 11674180), PCSIRT (IRT_13R29) and 111 Project (No. B07013) in China, and the Institute for Basic Science in Korea (IBS-R024-D1 and IBS-R024-Y1).

*songdaohong@nankai.edu.cn
†dleykam@ibs.re.kr
‡sflach@ibs.re.kr
§zgchen@nankai.edu.cn
‖Present address: Department of Physics, Indian Institute of Science Education and Research (IISER) Bhopal, Madhya Pradesh 462066, India.

[1] E. H. Lieb, Phys. Rev. Lett. **62**, 1201 (1989).
[2] A. Mielke, J. Phys. A **24**, 3311 (1991); **25**, 4335 (1992).
[3] H. Tasaki, Eur. Phys. J. B **64**, 365 (2008).
[4] F. Baboux *et al.*, Phys. Rev. Lett. **116**, 066402 (2016).
[5] W. Maimait, A. Andreanov, H. C. Park, O. Gendelman, and S. Flach, Phys. Rev. B **95**, 115135 (2017).
[6] M. Goda, S. Nishino, and H. Matsuda, Phys. Rev. Lett. **96**, 126401 (2006).
[7] M. Hyrkäs, V. Apaja, and M. Manninen, Phys. Rev. A **87**, 023614 (2013).
[8] S. D. Huber and E. Altman, Phys. Rev. B **82**, 184502 (2010).
[9] V. Apaja, M. Hyrkäs, and M. Manninen, Phys. Rev. A **82**, 041402 (2010).
[10] D. Green, L. Santos, and C. Chamon, Phys. Rev. B **82**, 075104 (2010).
[11] C. Weeks and M. Franz, Phys. Rev. B **82**, 085310 (2010).
[12] D. L. Bergman, C. Wu, and L. Balents, Phys. Rev. B **78**, 125104 (2008).
[13] D. Leykam, S. Flach, O. Bahat-Treidel, and A. S. Desyatnikov, Phys. Rev. B **88**, 224203 (2013).
[14] J. T. Chalker, T. S. Pickles, and P. Shukla, Phys. Rev. B **82**, 104209 (2010).
[15] E. J. Bergholtz and Z. Liu, Int. J. Mod. Phys. B **27**, 1330017 (2013).
[16] S. A. Parameswaran, R. Roy, and S. L. Sondhi, Physique **14**, 816 (2013).
[17] T. Neupert, L. Santos, C. Chamon, and C. Mudry, Phys. Rev. Lett. **106**, 236804 (2011).
[18] K. Sun, Z. Gu, H. Katsura, and S. Das Sarma, Phys. Rev. Lett. **106**, 236803 (2011).
[19] E. Tang, J.-W. Mei, and X.-G. Wen, Phys. Rev. Lett. **106**, 236802 (2011).
[20] S. Peotta and P. Törmä, Nat. Commun. **6**, 8944 (2015).
[21] A. Julku, S. Peotta, T. I. Vanhala, D.-H. Kim, and P. Törmä, Phys. Rev. Lett. **117**, 045303 (2016).

[22] R. Shen, L. B. Shao, B. Wang, and D. Y. Xing, Phys. Rev. B **81**, 041410(R) (2010).
[23] A. Ramachandran, A. Andreanov, and S. Flach, Phys. Rev. B **96**, 161104(R) (2017).
[24] S. Taie, H. Ozawa, T. Ichinose, T. Nishio, S. Nakajima, and Y. Takahashi, Sci. Adv. **1**, e1500854 (2015).
[25] W.-X. Qiu, S. Li, J.-H. Gao, Y. Zhou, and F.-C. Zhang, Phys. Rev. B **94**, 241409 (2016).
[26] M. R. Slot, T. S. Gardenier, P. H. Jacobse, G. C. P. van Miert, S. N. Kempkes, S. J. M. Zevenhuizen, C. M. Smith, D. Vanmaekelbergh, and I. Swart, Nat. Phys. **13**, 672 (2017).
[27] S. Klembt, T. H. Harder, O. A. Egorov, K. Winkler, H. Suchomel, J. Beierlein, M. Emmerling, C. Schneider, and S. Höfling, Appl. Phys. Lett. **111**, 231102 (2017); C. E. Whittaker *et al.*, Phys. Rev. Lett. **120**, 097401 (2018).
[28] F. Diebel, D. Leykam, S. Kroesen, C. Denz, and A. S. Desyatnikov, Phys. Rev. Lett. **116**, 183902 (2016).
[29] D. Guzmán-Silva, C. Mejía-Cortés, M. A. Bandres, M. C. Rechtsman, S. Weimann, S. Nolte, M. Segev, A. Szameit, and R. A. Vicencio, New J. Phys. **16**, 063061 (2014).
[30] R. A. Vicencio, C. Cantillano, L. Morales-Inostroza, B. Real, C. Mejía-Cortés, S. Weimann, A. Szameit, and M. I. Molina, Phys. Rev. Lett. **114**, 245503 (2015).
[31] S. Mukherjee, A. Spracklen, D. Choudhury, N. Goldman, P. Öhberg, E. Andersson, and R. R. Thomson, Phys. Rev. Lett. **114**, 245504 (2015).
[32] S. Xia, Y. Hu, D. Song, Y. Zong, L. Tang, and Z. Chen, Opt. Lett. **41**, 1435 (2016).
[33] F. Lederer, G. I. Stegeman, D. N. Christodoulides, G. Assanto, M. Segev, and Y. Silberberg, Phys. Rep. **463**, 1 (2008).
[34] C. W. Hsu, B. Zhen, A. D. Stone, J. D. Joannopoulos, and M. Soljačić, Nat. Rev. Mater. **1**, 16048 (2016).
[35] D. C. Marinica, A. G. Borisov, and S. V. Shabanov, Phys. Rev. Lett. **100**, 183902 (2008).
[36] Y. Plotnik, O. Peleg, F. Dreisow, M. Heinrich, S. Nolte, A. Szameit, and M. Segev, Phys. Rev. Lett. **107**, 183901 (2011).
[37] Y. Plotnik *et al.*, Nat. Mater. **13**, 57 (2014).
[38] See Supplemental Material at http://link.aps.org/supplemental/10.1103/PhysRevLett.121.263902 for edge-dependent CLS superposition and necklace-shaped flatband states in Lieb lattices.
[39] F. Diebel, P. Rose, M. Boguslawski, and C. Denz, Appl. Phys. Lett. **104**, 191101 (2014).
[40] R. A. Vicencio and C. Mejía-Cortés, J. Opt. **16**, 015706 (2014).
[41] C. Li, F. Ye, X. Chen, Y. V. Kartashov, A. Ferrando, L. Torner, and D. V. Skryabin, Phys. Rev. B **97**, 081103(R) (2018).
[42] R. Chen, D.-H. Xu, and B. Zhou, Phys. Rev. B **96**, 205304 (2017).
[43] J. Noh, S. Huang, K. P. Chen, and M. C. Rechtsman, Phys. Rev. Lett. **120**, 063902 (2018).
[44] J. Rhim and B. Yang, arXiv:1808.05926.